Predicting Ultrahigh-Energy Neutrino Events in IceCube

Sam Glosser* and Advisor: Joanna Kiryluk
Stony Brook University

(Dated: December 5, 2022)

An analytical approach for predicting the rate of neutrino events detected by the IceCube Neutrino Observatory is explored and implemented using Python. Developing a model for attenuation due to the earth and combining existing models for neutrino cross sections and differential flux, the number of neutrinos of a given flavor from astrophysical and atmospheric sources can be computed. These computations can be configured to focus on specific energy and zenith angle ranges, and the package allows the underlying mathematical models to be adjusted or entirely replaced as needed.

I. INTRODUCTION

Located deep in the South Pole, the IceCube Neutrino Observatory measures neutrino flux from atmospheric and astrophysical sources. To do this, digital sensors are used to pick up the light emitted when a neutrino collides with a nucleon within a large ($1\,\mathrm{km}^3$) volume of ice. [1]

To predict the number of ultrahigh-energy ($E \geq 1\,\mathrm{TeV}$) neutrino collision events in IceCube per year, I developed a Python package `NeutrinoFlux` that implements the approach discussed in this paper.

II. THEORETICAL BACKGROUND

We start with a spherical coordinate system centered on the south pole where our detector is; we approximate the detector as a single point at the origin as it is very small relative to the earth itself.

Flux from angles $\theta \in [0, \theta/2)$ will have to pass through the earth a total distance of $x(\theta) = 2R_E \cos\theta$, where R_E is the radius of the earth, which will attenuate it by some amount. The amount of attenuation increases with the mass density of the earth, but the mass density depends on the radial distance from the earth's core. So first, we need to compute this radius r in terms of θ and the distance $z \in [0, x(\theta)]$ that has been penetrated at any given time.

Based on Figure 1, the law of cosines gives

$$r^2 = R_E^2 + [x - z]^2 - 2R_E[x - z]\cos\theta,$$

so substituting $x = 2R_E\cos\theta$ into the last term, we get

$$r(z, \theta) = \sqrt{R_E^2 + [x(\theta) - z]^2 - 2x(\theta)[x(\theta) - z]}. \quad (1)$$

A. Detector

Since nucleons make up effectively all of the mass in any substance, they have a volumetric number density in ice of about

$$\rho_{N,\mathrm{ice}} = \frac{d_{\mathrm{ice}}}{m_N} \approx 5.48 \times 10^{29}\,\mathrm{m}^{-3}, \quad (2)$$

where $m_N = 1.67 \times 10^{-24}\,\mathrm{g}$ is the mass of a nucleon and $d_{\mathrm{ice}} = 916.9 \times 10^3\,\mathrm{g/m}^3$ is the density of ice.

With this, the rate of νN (or $\bar{\nu} N$) events in the detector for a given flavor is [2]

$$\mathrm{rate} = \rho_{N,\mathrm{ice}} V \iint \sigma(E) \frac{dN}{dE}(E, \theta)\, dE\, d\Omega, \quad (3)$$

where $\sigma(E)$ is the total cross section for that flavor of (anti)neutrino, dN/dE is the differential flux reaching the detector, and $d\Omega$ is the differential solid angle

$$d\Omega = \sin\theta\, d\theta\, d\phi. \quad (4)$$

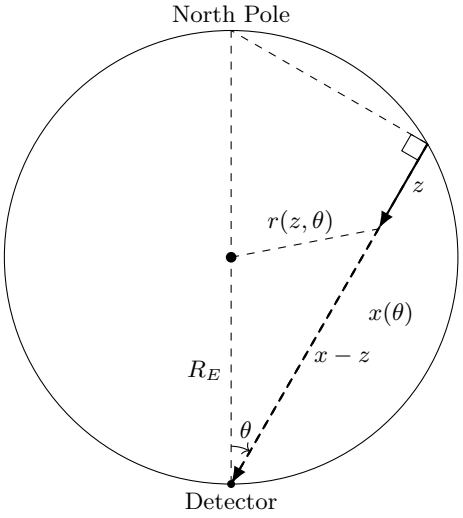

FIG. 1: Vertical cross section of the earth for a given azimuthal angle ϕ. Neutrino flux with zenith angle θ relative to the detector at the south pole penetrates the earth by an amount z and has to travel a total distance of $x(\theta) = 2R_E\cos\theta$ before reaching this detector. The mass density of the earth, which determines the attenuation of the flux, depends on the distance r from the center of the earth, which can in turn be computed via the law of cosines using θ, R_E, and the travel distance remaining $x(\theta) - z$.

* sam.glosser@stonybrook.edu

The differential flux is assumed to be constant in/averaged over ϕ while varying in E and possibly θ.

B. Attenuation

Suppose we send I_0 particles at a thick slab of matter of thickness x. From [3], the number of particles dI that get absorbed by a thin lamina of thickness dz at z is

$$dI(z) = -\sigma\rho(z)I(z)\,dz,$$

where σ is the total cross section and $\rho(z)$ is the volumetric number density of particles that absorb or scatter the incoming radiation. Solving this differential equation for I yields

$$I(x) = I_0 \exp\left(-\sigma\int_0^x \rho(z)\,dz\right), \tag{5}$$

where $I(x)/I_0$ is the attenuation factor, i.e. the fraction of particles that makes it through to x.

We apply this to the differential flux traveling towards the detector. Assuming the atmosphere is too thin to contribute significantly to attenuation, the only source of attenuation is from the earth itself. So, we write the cross section as $\sigma = \sigma(E)$, and the number density as

$$\rho_{N,\text{earth}}(z,\theta) = \frac{d_{\text{earth}}(z,\theta)}{m_N}, \tag{6}$$

Therefore, if the initial differential flux is $I_0 = \Phi(E,\theta)$, the final flux $dN/dE(E,\theta)$ will be

$$\frac{dN}{dE}(E,\theta) = \Phi(E,\theta)\cdot\exp\big[-m_N^{-1}\alpha(\theta)\sigma(E)\big], \tag{7}$$

where $\alpha(\theta)$ is the integral over the mass density

$$\alpha(\theta) \coloneqq \int_0^{x(\theta)} d_{\text{earth}}(r(z,\theta))\,dz. \tag{8}$$

Higher values of $\alpha(\theta)$ yield more attenuation; thus, we call α the attenuation parameter for a trajectory with zenith angle θ.

Using the Preliminary Earth Model [4], the mass density of the earth d_{earth} is a function of the radial distance r from the core:

$$d_{\text{earth}}(r) = \begin{cases} 13.0885 - 8.8381y^2 & r < 1221.5, \\ 12.5815 - 1.2638y - 3.6426y^2 - 5.5281y^3 & 1221.5 < r < 3480 \\ 7.9565 - 6.4761y + 5.5283y^2 - 3.0807y^3 & 3480 < r < 5701 \\ 5.3197 - 1.4836y & 5701 < r < 5771 \\ 11.2494 - 8.0298y & 5771 < r < 5971 \\ 7.1089 - 3.8045y & 5971 < r < 6151 \\ 2.691 + 0.6924y & 6151 < r < 6346.6 \\ 2.9 & 6346.6 < r < 6356 \\ 2.6 & 6356 < r < 6368 \\ 1.02 & r \le R_E. \end{cases} \tag{9}$$

Here, r is measured in km, $y \coloneqq R/R_E$ is a dimensionless parameter, $R_E = 6371\,\text{km}$ is the radius of the earth, and d_{earth} is measured in g/cm^3.

C. Cross Sections

Neutrinos and antineutrinos have two primary types of interactions with nucleons: charged-current (CC) and neutral-current (NC). Each interaction has a cross section $\sigma_{\text{CC}}(E)$ or $\sigma_{\text{NC}}(E)$ associated with it, which can be computed using pertubative QCD [2].

Furthermore, at energies close to 6.3 PeV (more specifically, between 4 and 8 PeV), W bosons are formed in electron antineutrino collisions $\bar{\nu}_e + e^- \to W^-$; this process is known as Glashow Resonance.

If we assume that $\mu^2 - m_e^2 \ll 2m_eE$ for the energy range we are using, we can approximate the differential cross section of these collisions as [2] [5]

$$\frac{d\sigma_{\text{GR}}}{dy}(E) = \frac{\Gamma(W\to\text{hadrons})}{\Gamma(W\to\mu\bar{\nu}_\mu)}\cdot\frac{G_F^2 m_e E}{2\pi}\frac{4(1-y)^2[1-\cancel{(\mu^2-m_e^2)^2/2m_eE}]^2}{(1-2mE/M_W^2)^2+\Gamma_W^2/M_W^2}.$$

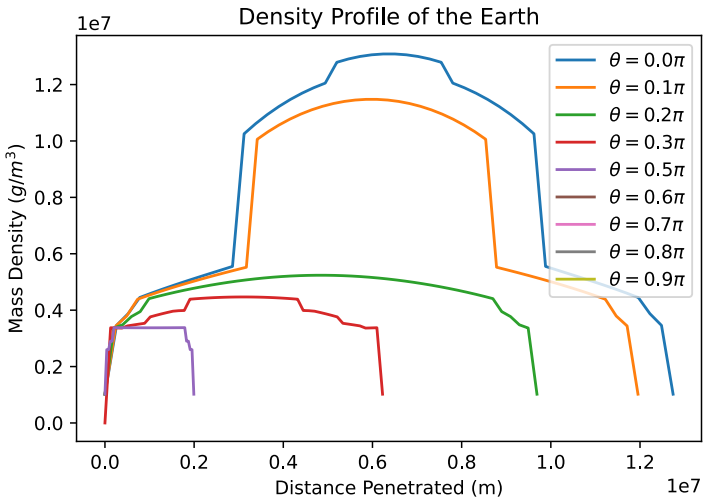

FIG. 2: The nucleon number density in the earth as a function of the flux penetration distance z for varying zenith angles θ. The $\theta = 0$ plot shows how the density of the earth increases as the flux gets closer to the core, and decreases when moving away from it. Thus, as θ increases, the flux's trajectory gets closer to the surface and meets less dense material along it, and has a smaller distance $x(\theta)$ to travel in total.

Thus, if we define the constants

$$\sigma_0 := \frac{G_F^2 M_W^2}{\pi(\hbar c)^2}, \quad S_W := \frac{2m_e}{M_W^2}E, \quad R_{W,\mu} = \frac{\Gamma(W \to \mu\bar{\nu}_\mu)}{\Gamma(W \to \text{hadrons})}, \quad G_W := \frac{\Gamma_W}{M_W} \tag{10}$$

where $(\hbar c)^2$ is used as a conversion factor, we get

$$\sigma_{\text{GR}}(E) = \int_0^1 \frac{d\sigma_{\text{GR}}}{dy} dy = \frac{\sigma_0}{3R_{W,\mu}} \frac{S_W}{(1-S_W)^2 + G_W^2}. \tag{11}$$

The relevant constants are shown in Table I. A plot of $\sigma_{\text{GR}}(E)$ is shown in Figure 3.

Name	Value
G_F	$1.166\,38 \times 10^{-5}\,\text{GeV}^2$
m_e	$5.109\,99 \times 10^{-4}\,\text{GeV/c}^2$
M_W	$80.379\,\text{GeV/c}^2$
$R_{W,\mu}$	0.1057
G_W	0.026 34
$(\hbar c)^2$	$0.389\,38\,\text{GeV}^2\text{mbarn}$

TABLE I: The relevant constants used in (11) to compute $\sigma_{\text{GR}}(E)$. [2] [6].

From here, we consider the number density of targets for Glashow Resonance, i.e. electrons. Water has 10 electrons for every 18 nucleons. Meanwhile, we assume the earth is made of heavier elements whose mass is more evenly distributed between protons and neutrons; thus, since the number of protons and electrons are equal, the earth has roughly 1 electron for every 2 nucleons. This gives a total event rate for $\bar{\nu}_e$ of

$$\begin{aligned}\text{rate} &= V \iint \left[\rho_{N,\text{ice}}\sigma(E) + \rho_{e,\text{ice}}\sigma_{\text{GR}}(E)\right] \frac{dN}{dE}(E,\theta)\, dE\, d\Omega \\ &= \rho_{N,\text{ice}} V \iint \left[\sigma(E) + \frac{10}{18}\sigma_{\text{GR}}(E)\right] \frac{dN}{dE}(E,\theta)\, dE\, d\Omega,\end{aligned} \tag{12}$$

where the attenuated differential flux is now

$$\frac{dN}{dE}(E,\theta) = \Phi(E,\theta) \exp\left(-m_N^{-1}\alpha(\theta)\left[\sigma(E) + \frac{1}{2}\sigma_{\text{GR}}(E)\right]\right). \tag{13}$$

D. Flux Sources

We consider two sources of differential flux: astrophysical flux from space, and atmospheric flux generated from a multitude of particle interactions in the sky.

Astrophysical flux is a diffuse, isotropic flux of neutri-

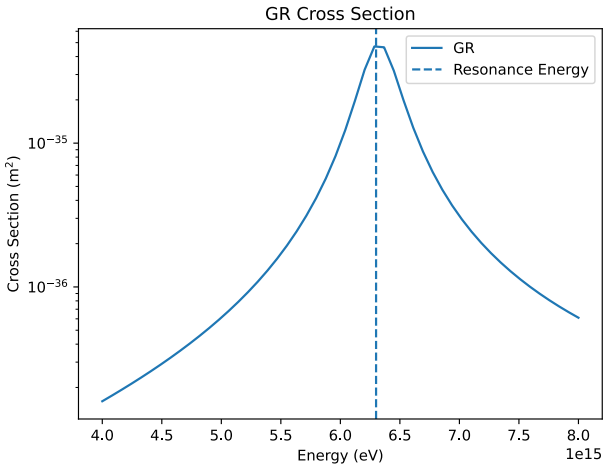

FIG. 3: Plot of $\sigma_{\mathrm{GR}}(E)$ for $\bar{\nu}_e$ within its domain $4\,\mathrm{PeV} \leq E \leq 8\,\mathrm{PeV}$, with the resonance peak at about $E_{\mathrm{res}} = 6.3\,\mathrm{PeV}$.

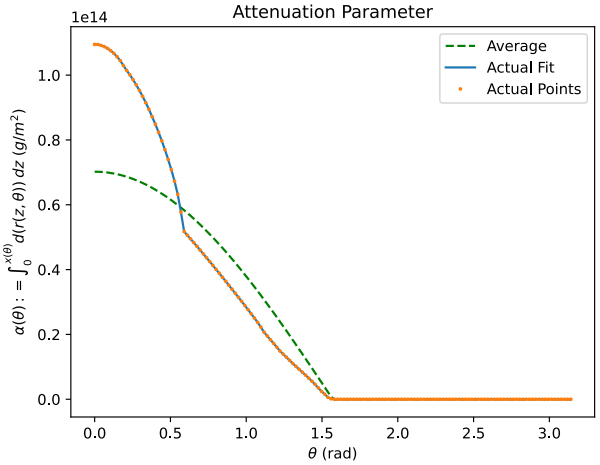

FIG. 4: The attenuation parameter α as a function of the zenith angle θ of the incoming differential flux. The green line is the α parameter obtained by replacing the earth density (9) with its average density $5.51\,\mathrm{g/cm^3}$; as expected from Figure 2, trajectories closer to the earth's core (with low θ) meet denser-than-average material and experience more attenuation compared to those that are far from it (high θ). Flux with a zenith angle in the interval $[\pi/2, \pi]$ experiences no attenuation ($\alpha = 0$), as those particles do not pass through the earth at all.

nos of interstellar origin that can be modeled as [7]:

$$\Phi^{\nu}_{\mathrm{astro}}(E) = \Phi^{\bar{\nu}}_{\mathrm{astro}}(E) = \frac{1}{2} C_0 \phi_{\mathrm{astro}} \left(E/E_0\right)^{-\gamma}. \quad (14)$$

Here, $C_0 = 3{\times}10^{-18}\,\mathrm{GeV^{-1}cm^{-2}s^{-1}sr^{-1}}$, $E_0 = 100\,\mathrm{TeV}$, $\phi_{\mathrm{astro}} = 1.66(27)$ is the normalization for each neutrino flavor, and $\gamma = 2.53(7)$ is the flux spectral index. The $1/2$ is included so that $\Phi^{\nu}_{\mathrm{astro}}$ and $\Phi^{\bar{\nu}}_{\mathrm{astro}}$, which are assumed to be equivalent in [7], can be considered separately.

Meanwhile, atmospheric neutrino is produced in air showers when cosmic rays interact with particles in the earth's atmosphere. Conventional atmospheric flux dominates at lower energy ranges and is produced by the decay of pions and kaons, while prompt neutrino flux comes from the decay of heavier mesons [8] [9].

This differential flux depends on both the energy E and the zenith angle θ, and is described by a set of matrix cascade equations [10] that won't be covered here.

III. IMPLEMENTATION

I developed a Python package `NeutrinoFlux` that implements the functions for the cross sections, the attenuation parameter, and the differential flux sources individually, and then puts them all together to acquire the yearly rate (3) (or (12)).

The majority of these functions are implemented using NumPy for mathematical functions and array manipulation [11], SciPy for interpolation and numerical integration [12], and Matplotlib to create the plots shown in this paper [13]. Furthermore, the MCEq package [14] is used to acquire the atmospheric flux, as decribed in the differential flux section below.

A. Attenuation

As shown in Figure 4, the function for $\alpha(\theta)$ was computed for a spread of angles $\theta \in [0, \pi]$, and a 1-D interpolated spline was used to fill in the remainder of the interval.

Furthermore, a typical plot of the attenuation exponential $(dN/dE)/\Phi$ is shown in Figure 5, with selected data presented in Table II.

	E (eV)				
$\cos\theta$	10^{14}	10^{15}	10^{16}	10^{17}	10^{18}
0.2	0.867	0.623	0.264	0.035	0
0.3	0.802	0.483	0.129	0.006	0
0.4	0.731	0.354	0.054	0.001	0
0.5	0.647	0.237	0.017	0	0
0.6	0.572	0.158	0.006	0	0
0.7	0.502	0.102	0.002	0	0
0.8	0.435	0.064	0	0	0

TABLE II: A table of attenuation factors from Figure 5, rounded to three decimal places.

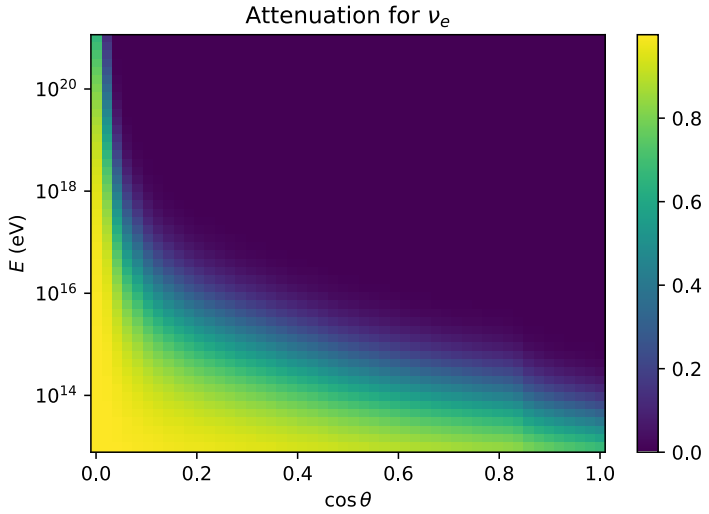

FIG. 5: A plot of the attenuation factor $(dN/dE)/\Phi$ for ν_e with respect to E and $\cos\theta$. As expected, the amount of attenuation is strengthened when $\cos\theta$ increases (i.e. θ decreases) and when E increases. Notice that for energies above 10^{18}eV or so, the flux is almost entirely blocked for any angle where $\cos\theta > 0.1$.

B. Cross Sections

Using the same scheme, the cross section tables from [15] were interpolated to acquire $\sigma_{\text{CC}}(E)$ and $\sigma_{\text{NC}}(E)$, as shown in Figure 6a and 6b. Note that these plots are consistent with the older plots found in [2].

C. Atmospheric Flux

For the atmospheric flux, there exists a package MCEq that solves these cascade equations for a given θ, yielding the differential flux for a variety of energies E. I used this package to solve the system for a spread of angles and used a 2-D rectangular interpolating spline is used to acquire $\Phi_{\text{atmo}}(E, \theta)$ for all E and θ in our domain of consideration [14].

IV. RESULTS

We concentrate on results for electron neutrinos ν_e and $\bar{\nu}_e$ due to limitations discussed in the Conclusion section.

The yearly rates for electron neutrinos and antineutrinos are shown in Table III. Of the $\bar{\nu}_e$ events, about 1 of them per year comes from Glashow Resonance within the detector, stemming from astrophysical flux with $\theta \in [\pi/2, \pi]$. This makes sense, as the large cross section for σ_{GR} blocks most of the flux around the resonance energy peak while passing through the earth.

Using MCEq, we can split the atmospheric neutrinos according to their flux sources. For example, for the atmospheric ν_e and $\bar{\nu}_e$ with $\theta \in [0, \pi]$, we acquire the results in Table IV.

	$[0, \pi/2)$		$[\pi/2, \pi]$	
	Astro	Atmo	Astro	Atmo
ν_e	52	21	66	24
$\bar{\nu}_e$	40	13	51	15

TABLE III: The yearly rates for ν_e and $\bar{\nu}_e$ events with energies between 10^{13} and 10^{21} eV for both astrophysical and atmospheric flux. The rates are split between $\theta \in [0, \pi/2)$ and $\theta \in [\pi/2, \pi]$ to show the effects of attenuation. Atmospheric flux is evaluated assuming the month is January, with similar results for July.

	K	π	Conv.	Pr.	Tot.
ν_e	16	0.1	32.2	13.3	45.5
$\bar{\nu}_e$	7	0.08	19	10	29

TABLE IV: The yearly rates of atmospheric ν_e and $\bar{\nu}_e$ events with the month being January and $\theta \in [0, \pi]$, split between neutrinos from kaon, pion, conventional, prompt, and total sources [14].

We can also compare the results acquired by the parameters used for our astrophysical flux law. For example, when we instead use baseline fit parameters of $\gamma = 2$ and $\phi_{\text{astro}} = 1$ in (14), we get the results in Table V. Of the $\bar{\nu}_e$ events here, about 6 of them (all from the range $\theta \in [\pi/2, \pi]$, as before) are Glashow Resonance events.

As another example of results that can be obtained from the `NeutrinoFlux` package, Figure 7 displays the total event rate for ν_e and $\bar{\nu}_e$ in the energy range $[10\,\text{TeV}, E]$ as a function of E.

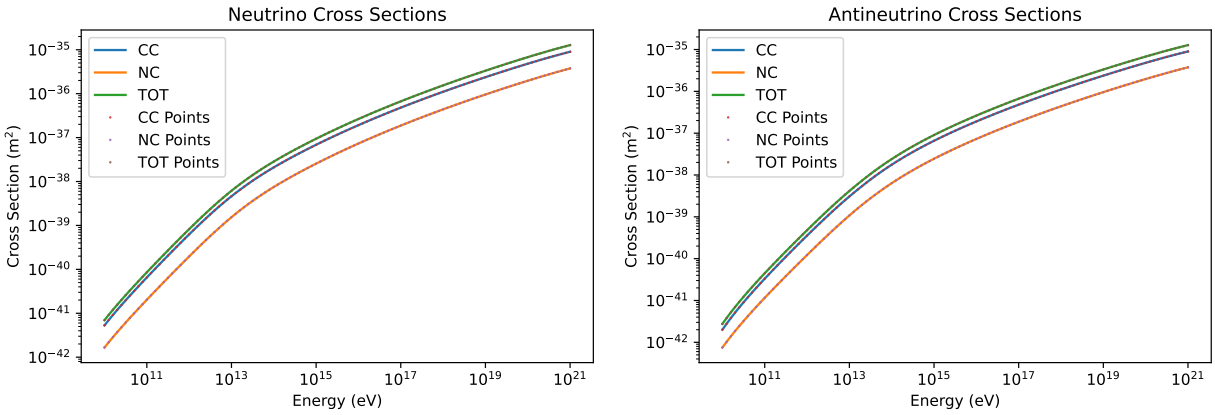

(a) Plots of $\sigma_{\mathrm{CC}}(E)$ and $\sigma_{\mathrm{NC}}(E)$, and their sum $\sigma(E)$, for ν.

(b) Plots of $\sigma_{\mathrm{CC}}(E)$ and $\sigma_{\mathrm{NC}}(E)$, and their sum $\sigma(E)$, for $\bar{\nu}$.

FIG. 6: Plots of the charged-current and neutral-current cross sections for neutrinos and antineutrinos. being used to compute the event rate in the detector. For each plot, a 1-D interpolating spline is used to connect the data points computed in [15].

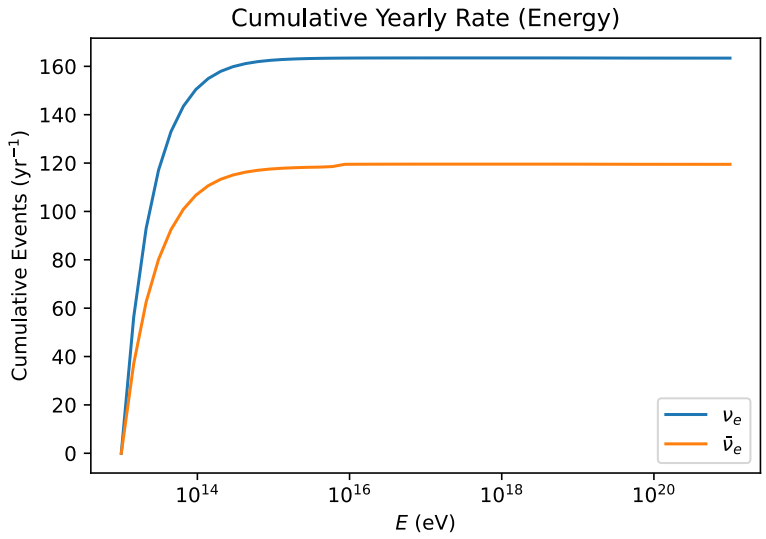

FIG. 7: Plot of the total yearly events for ν_e and $\bar{\nu}_e$ particles between 10^{13} eV and E. Consistent with the discussion of Figure 5 (and (14)'s decay model), the contribution from neutrinos above 10^{18} eV or so are negligible. The small jump in $\bar{\nu}_e$ events before 10^{16} eV corresponds to Glashow Resonance events near $E_{\mathrm{res}} = 6.3\,\mathrm{PeV}$.

	$[0, \pi/2)$	$[\pi/2, \pi]$
ν_e	17	25
$\bar{\nu}_e$	14	26

TABLE V: The yearly rates for ν_e and $\bar{\nu}_e$ events with energies between 10^{13} and 10^{21} eV from astrophysical flux, but with modified fit parameters $\gamma = 2$ and $\phi_{\mathrm{astro}} = 1$ used for the differential flux (14).

V. CONCLUSIONS

Equations (3) and (12) were successfully implemented in Python, allowing for the theoretical rate of astrophysical and atmospheric neutrinos detected by IceCube to be computed. This computation can be done individually for specific neutrino flavors, flux sources, within specified energy and angle bounds.

The results acquired are limited primarily by inaccuracies in the models used. For example, the attenuation of τ neutrinos doesn't account for the production of secondary neutrinos during its propagation through the

earth [16], which decreases the effective attenuation of all three neutrino flavors.

As another example, while the month of the year for atmospheric flux can be configured, the only options are January and July, and the yearly rate is computed assuming the month stays constant for the whole year. A more accurate model would replace $\Phi(E, \theta)$ with a time-dependent function $\Phi(E, \theta, t)$ and integrate over the course of a year to acquire the desired rate.

Fortunately, the `NeutrinoFlux` package was designed with potential solutions to some of these issues in mind. Using an object-oriented approach, the package is centered around a custom `Neutrino` Python class, where each neutrino object has attributes for its cross sections, attenuation factor, and differential flux as functions of the appropriate variables. While these objects use the models discussed in this paper by default, it is possible to replace or modify these attributes to incorporate new models as appropriate.

For example, the `nuFATE` package can be used to compute the attenuation factor for neutrino flux, including contributions from ν_τ regeneration effects [16]. If one were to create functions for the attenuation parameter of each neutrino type in terms of E and θ using `nuFATE`, the `attenuation` attribute of a `Neutrino` object from `NeutrinoFlux` could then be modified to call that function instead of the one in this paper.

While robust simulations using event generators such as `PYTHIA` do exist, it is still hoped that the more analytical approach presented in this paper is of some value.

[1] M. Aartsen, M. Ackermann, J. Adams, J. Aguilar, M. Ahlers, M. Ahrens, D. Altmann, K. Andeen, T. Anderson, I. Ansseau, G. Anton, M. Archinger, C. Argüelles, R. Auer, J. Auffenberg, S. Axani, J. Baccus, X. Bai, S. Barnet, S. Barwick, V. Baum, R. Bay, K. Beattie, J. Beatty, J. B. Tjus, K.-H. Becker, T. Bendfelt, S. BenZvi, D. Berley, E. Bernardini, A. Bernhard, D. Besson, G. Binder, D. Bindig, M. Bissok, E. Blaufuss, S. Blot, D. Boersma, C. Bohm, M. Börner, F. Bos, D. Bose, S. Böser, O. Botner, A. Bouchta, J. Braun, L. Brayeur, H.-P. Bretz, S. Bron, A. Burgman, C. Burreson, T. Carver, M. Casier, E. Cheung, D. Chirkin, A. Christov, K. Clark, L. Classen, S. Coenders, G. Collin, J. Conrad, D. Cowen, R. Cross, C. Day, M. Day, J. de André, C. D. Clercq, E. del Pino Rosendo, H. Dembinski, S. D. Ridder, F. Descamps, P. Desiati, K. de Vries, G. de Wasseige, M. de With, T. DeYoung, J. Díaz-Vélez, V. di Lorenzo, H. Dujmovic, J. Dumm, M. Dunkman, B. Eberhardt, W. Edwards, T. Ehrhardt, B. Eichmann, P. Eller, S. Euler, P. Evenson, S. Fahey, A. Fazely, J. Feintzeig, J. Felde, K. Filimonov, C. Finley, S. Flis, C.-C. Fösig, A. Franckowiak, M. Frère, E. Friedman, T. Fuchs, T. Gaisser, J. Gallagher, L. Gerhardt, K. Ghorbani, W. Giang, L. Gladstone, T. Glauch, D. Glowacki, T. Glüsenkamp, A. Goldschmidt, J. Gonzalez, D. Grant, Z. Griffith, L. Gustafsson, C. Haack, A. Hallgren, F. Halzen, E. Hansen, T. Hansmann, K. Hanson, J. Haugen, D. Hebecker, D. Heereman, K. Helbing, R. Hellauer, R. Heller, S. Hickford, J. Hignight, G. Hill, K. Hoffman, R. Hoffmann, K. Hoshina, F. Huang, M. Huber, P. Hulth, K. Hultqvist, S. In, M. Inaba, A. Ishihara, E. Jacobi, J. Jacobsen, G. Japaridze, M. Jeong, K. Jero, A. Jones, B. Jones, J. Joseph, W. Kang, A. Kappes, T. Karg, A. Karle, U. Katz, M. Kauer, A. Keivani, J. Kelley, J. Kemp, A. Kheirandish, J. Kim, M. Kim, T. Kintscher, J. Kiryluk, N. Kitamura, T. Kittler, S. Klein, S. Kleinfelder, M. Kleist, G. Kohnen, R. Koirala, H. Kolanoski, R. Konietz, L. Köpke, C. Kopper, S. Kopper, D. Koskinen, M. Kowalski, M. Krasberg, K. Krings, M. Kroll, G. Krückl, C. Krüger, J. Kunnen, S. Kunwar, N. Kurahashi, T. Kuwabara, M. Labare, K. Laihem, H. Landsman, J. Lanfranchi, M. Larson, F. Lauber, A. Laundrie, D. Lennarz, H. Leich, M. Lesiak-Bzdak, M. Leuermann, L. Lu, J. Ludwig, J. Lünemann, C. Mackenzie, J. Madsen, G. Maggi, K. Mahn, S. Mancina, M. Mandelartz, R. Maruyama, K. Mase, H. Matis, R. Maunu, F. McNally, C. McParland, P. Meade, K. Meagher, M. Medici, M. Meier, A. Meli, T. Menne, G. Merino, T. Meures, S. Miarecki, R. Minor, T. Montaruli, M. Moulai, T. Murray, R. Nahnhauer, U. Naumann, G. Neer, M. Newcomb, H. Niederhausen, S. Nowicki, D. Nygren, A. O. Pollmann, A. Olivas, A. O'Murchadha, T. Palczewski, H. Pandya, D. Pankova, S. Patton, P. Peiffer, O. Penek, J. Pepper, C. P. de los Heros, C. Pettersen, D. Pieloth, E. Pinat, P. Price, G. Przybylski, M. Quinnan, C. Raab, L. Rädel, M. Rameez, K. Rawlins, R. Reimann, B. Relethford, M. Relich, E. Resconi, W. Rhode, M. Richman, B. Riedel, S. Robertson, M. Rongen, C. Roucelle, C. Rott, T. Ruhe, D. Ryckbosch, D. Rysewyk, L. Sabbatini, S. S. Herrera, A. Sandrock, J. Sandroos, P. Sandstrom, S. Sarkar, K. Satalecka, P. Schlunder, T. Schmidt, S. Schoenen, S. Schöneberg, A. Schukraft, L. Schumacher, D. Seckel, S. Seunarine, M. Solarz, D. Soldin, M. Song, G. Spiczak, C. Spiering, T. Stanev, A. Stasik, J. Stettner, A. Steuer, T. Stezelberger, R. Stokstad, A. Stößl, R. Ström, N. Strotjohann, K.-H. Sulanke, G. Sullivan, M. Sutherland, H. Taavola, I. Taboada, J. Tatar, F. Tenholt, S. Ter-Antonyan, A. Terliuk, G. Tešić, L. Thollander, S. Tilav, P. Toale, M. Tobin, S. Toscano, D. Tosi, M. Tselengidou, A. Turcati, E. Unger, M. Usner, J. Vandenbroucke, N. van Eijndhoven, S. Vanheule, M. van Rossem, J. van Santen, M. Vehring, M. Voge, E. Vogel, M. Vraeghe, D. Wahl, C. Walck, A. Wallace, M. Wallraff, N. Wandkowsky, C. Weaver, M. Weiss, C. Wendt, S. Westerhoff, D. Wharton, B. Whelan, S. Wickmann, K. Wiebe, C. Wiebusch, L. Wille, D. Williams, L. Wills, P. Wisniewski, M. Wolf, T. Wood, E. Woolsey, K. Woschnagg, D. Xu, X. Xu, Y. Xu, J. Yanez, G. Yodh, S. Yoshida, and M. Zoll, The IceCube neutrino observatory: instrumentation and online systems, Journal of Instrumentation **12** (03), P03012.

[2] R. Gandhi, C. Quigg, M. H. Reno, and I. Sarcevic, Ultrahigh-energy neutrino interactions, Astroparticle Physics **5**, 81 (1996).

[3] R. Eisberg, R. Resnick, and J. D. Sullivan, Quantum physics of atoms, molecules, solids, nu-

clei and particles, Physics Today **28**, 51 (1975), https://doi.org/10.1063/1.3069243.

[4] A. M. Dziewonski and D. L. Anderson, Preliminary reference earth model, Physics of the Earth and Planetary Interiors **25**, 297 (1981).

[5] S. L. Glashow, Resonant scattering of antineutrinos, Phys. Rev. **118**, 316 (1960).

[6] R. L. Workman and Others (Particle Data Group), Review of Particle Physics, PTEP **2022**, 083C01 (2022).

[7] M. G. Aartsen, M. Ackermann, J. Adams, J. A. Aguilar, M. Ahlers, M. Ahrens, C. Alispach, K. Andeen, T. Anderson, I. Ansseau, G. Anton, C. Argüelles, J. Auffenberg, S. Axani, P. Backes, H. Bagherpour, X. Bai, A. Balagopal V., A. Barbano, S. W. Barwick, B. Bastian, V. Baum, S. Baur, R. Bay, J. J. Beatty, K.-H. Becker, J. Becker Tjus, S. BenZvi, D. Berley, E. Bernardini, D. Z. Besson, G. Binder, D. Bindig, E. Blaufuss, S. Blot, C. Bohm, S. Böser, O. Botner, J. Böttcher, E. Bourbeau, J. Bourbeau, F. Bradascio, J. Braun, S. Bron, J. Brostean-Kaiser, A. Burgman, J. Buscher, R. S. Busse, T. Carver, C. Chen, E. Cheung, D. Chirkin, S. Choi, K. Clark, L. Classen, A. Coleman, G. H. Collin, J. M. Conrad, P. Coppin, P. Correa, D. F. Cowen, R. Cross, P. Dave, C. De Clercq, J. J. DeLaunay, H. Dembinski, K. Deoskar, S. De Ridder, P. Desiati, K. D. de Vries, G. de Wasseige, M. de With, T. DeYoung, A. Diaz, J. C. Díaz-Vélez, H. Dujmovic, M. Dunkman, E. Dvorak, B. Eberhardt, T. Ehrhardt, P. Eller, R. Engel, P. A. Evenson, S. Fahey, A. R. Fazely, J. Felde, K. Filimonov, C. Finley, D. Fox, A. Franckowiak, E. Friedman, A. Fritz, T. K. Gaisser, J. Gallagher, E. Ganster, S. Garrappa, L. Gerhardt, K. Ghorbani, T. Glauch, T. Glüsenkamp, A. Goldschmidt, J. G. Gonzalez, D. Grant, T. Grégoire, Z. Griffith, S. Griswold, M. Günder, M. Gündüz, C. Haack, A. Hallgren, R. Halliday, L. Halve, F. Halzen, K. Hanson, A. Haungs, D. Hebecker, D. Heereman, P. Heix, K. Helbing, R. Hellauer, F. Henningsen, S. Hickford, J. Hignight, G. C. Hill, K. D. Hoffman, R. Hoffmann, T. Hoinka, B. Hokanson-Fasig, K. Hoshina, F. Huang, M. Huber, T. Huber, K. Hultqvist, M. Hünnefeld, R. Hussain, S. In, N. Iovine, A. Ishihara, M. Jansson, G. S. Japaridze, M. Jeong, K. Jero, B. J. P. Jones, F. Jonske, R. Joppe, D. Kang, W. Kang, A. Kappes, D. Kappesser, T. Karg, M. Karl, A. Karle, U. Katz, M. Kauer, J. L. Kelley, A. Kheirandish, J. Kim, T. Kintscher, J. Kiryluk, T. Kittler, S. R. Klein, R. Koirala, H. Kolanoski, L. Köpke, C. Kopper, S. Kopper, D. J. Koskinen, M. Kowalski, K. Krings, G. Krückl, N. Kulacz, N. Kurahashi, A. Kyriacou, J. L. Lanfranchi, M. J. Larson, F. Lauber, J. P. Lazar, K. Leonard, M. Lesiak-Bzdak, A. Leszczyńska, M. Leuermann, Q. R. Liu, E. Lohfink, C. J. Lozano Mariscal, L. Lu, F. Lucarelli, J. Lünemann, W. Luszczak, Y. Lyu, W. Y. Ma, J. Madsen, G. Maggi, K. B. M. Mahn, Y. Makino, P. Mallik, K. Mallot, S. Mancina, I. C. Mariş, R. Maruyama, K. Mase, R. Maunu, F. McNally, K. Meagher, M. Medici, A. Medina, M. Meier, S. Meighen-Berger, G. Merino, T. Meures, J. Micallef, D. Mockler, G. Momenté, T. Montaruli, R. W. Moore, R. Morse, M. Moulai, P. Muth, R. Nagai, U. Naumann, G. Neer, H. Niederhausen, M. U. Nisa, S. C. Nowicki, D. R. Nygren, A. Obertacke Pollmann, M. Oehler, A. Olivas, A. O'Murchadha, E. O'Sullivan, T. Palczewski, H. Pandya, D. V. Pankova, N. Park, P. Peiffer, C. Pérez de los Heros, S. Philippen, D. Pieloth, S. Pieper, E. Pinat, A. Pizzuto, M. Plum, A. Porcelli, P. B. Price, G. T. Przybylski, C. Raab, A. Raissi, M. Rameez, L. Rauch, K. Rawlins, I. C. Rea, A. Rehman, R. Reimann, B. Relethford, M. Renschler, G. Renzi, E. Resconi, W. Rhode, M. Richman, S. Robertson, M. Rongen, C. Rott, T. Ruhe, D. Ryckbosch, D. Rysewyk, I. Safa, S. E. Sanchez Herrera, A. Sandrock, J. Sandroos, M. Santander, S. Sarkar, S. Sarkar, K. Satalecka, M. Schaufel, H. Schieler, P. Schlunder, T. Schmidt, A. Schneider, J. Schneider, F. G. Schröder, L. Schumacher, S. Sclafani, D. Seckel, S. Seunarine, S. Shefali, M. Silva, R. Snihur, J. Soedingrekso, D. Soldin, M. Song, G. M. Spiczak, C. Spiering, J. Stachurska, M. Stamatikos, T. Stanev, R. Stein, J. Stettner, A. Steuer, T. Stezelberger, R. G. Stokstad, A. Stößl, N. L. Strotjohann, T. Stürwald, T. Stuttard, G. W. Sullivan, I. Taboada, F. Tenholt, S. Ter-Antonyan, A. Terliuk, S. Tilav, K. Tollefson, L. Tomankova, C. Tönnis, S. Toscano, D. Tosi, A. Trettin, M. Tselengidou, C. F. Tung, A. Turcati, R. Turcotte, C. F. Turley, B. Ty, E. Unger, M. A. Unland Elorrieta, M. Usner, J. Vandenbroucke, W. Van Driessche, D. van Eijk, N. van Eijndhoven, J. van Santen, S. Verpoest, M. Vraeghe, C. Walck, A. Wallace, M. Wallraff, N. Wandkowsky, T. B. Watson, C. Weaver, A. Weindl, M. J. Weiss, J. Weldert, C. Wendt, J. Werthebach, B. J. Whelan, N. Whitehorn, K. Wiebe, C. H. Wiebusch, L. Wille, D. R. Williams, L. Wills, M. Wolf, J. Wood, T. R. Wood, K. Woschnagg, G. Wrede, D. L. Xu, X. W. Xu, Y. Xu, J. P. Yanez, G. Yodh, S. Yoshida, T. Yuan, and M. Zöcklein (IceCube Collaboration), Characteristics of the diffuse astrophysical electron and tau neutrino flux with six years of icecube high energy cascade data, Phys. Rev. Lett. **125**, 121104 (2020).

[8] A. Schukraft, A view of prompt atmospheric neutrinos with IceCube, Nuclear Physics B - Proceedings Supplements **237-238**, 266 (2013).

[9] R. Gauld, J. Rojo, L. Rottoli, S. Sarkar, and J. Talbert, The prompt atmospheric neutrino flux in the light of LHCb, Journal of High Energy Physics **2016**, 10.1007/jhep02(2016)130 (2016).

[10] R. Engel, F. Riehn, H. Dembinski, A. Fedynitch, T. Gaisser, and T. Stanev, The hadronic interaction model sibyll 2.3c and feynman scaling, in *Proceedings of 35th International Cosmic Ray Conference - PoS(ICRC2017)* (Sissa Medialab, 2017).

[11] C. R. Harris, K. J. Millman, S. J. van der Walt, R. Gommers, P. Virtanen, D. Cournapeau, E. Wieser, J. Taylor, S. Berg, N. J. Smith, R. Kern, M. Picus, S. Hoyer, M. H. van Kerkwijk, M. Brett, A. Haldane, J. F. del Río, M. Wiebe, P. Peterson, P. Gérard-Marchant, K. Sheppard, T. Reddy, W. Weckesser, H. Abbasi, C. Gohlke, and T. E. Oliphant, Array programming with NumPy, Nature **585**, 357 (2020).

[12] P. Virtanen, R. Gommers, T. E. Oliphant, M. Haberland, T. Reddy, D. Cournapeau, E. Burovski, P. Peterson, W. Weckesser, J. Bright, S. J. van der Walt, M. Brett, J. Wilson, K. J. Millman, N. Mayorov, A. R. J. Nelson, E. Jones, R. Kern, E. Larson, C. J. Carey, İ. Polat, Y. Feng, E. W. Moore, J. VanderPlas, D. Laxalde, J. Perktold, R. Cimrman, I. Henriksen, E. A. Quintero, C. R. Harris, A. M. Archibald, A. H. Ribeiro, F. Pedregosa, P. van Mulbregt, and SciPy 1.0 Contributors, SciPy 1.0: Fundamental Algorithms for Scientific Com-

puting in Python, Nature Methods **17**, 261 (2020).
[13] J. D. Hunter, Matplotlib: A 2d graphics environment, Computing in Science & Engineering **9**, 90 (2007).
[14] A. Fedynitch, R. Engel, T. K. Gaisser, F. Riehn, and T. Stanev, Calculation of conventional and prompt lepton fluxes at very high energy (2015).
[15] A. Cooper-Sarkar, P. Mertsch, and S. Sarkar, The high energy neutrino cross-section in the Standard Model and its uncertainty, JHEP **08**, 042, arXiv:1106.3723 [hep-ph].
[16] A. C. Vincent, C. A. Argüelles, and A. Kheirandish, High-energy neutrino attenuation in the earth and its associated uncertainties, Journal of Cosmology and Astroparticle Physics **2017** (11), 012.